Zonated quantification of immunohistochemistry in normal and steatotic livers

Manuscript title: Zonated quantification of immunohistochemistry in normal and steatotic livers

Short running title: Zonated immunohistochemistry in steatosis

Authors: Cédric Peleman* [1,2], Winnok Harald De Vos [3, 4, 5], Isabel Pintelon [3, 4, 5], Ann Driessen [6], Annelies Van Eyck [1], Christophe Van Steenkiste [1,2], Luisa Vonghia [1,2], Joris De Man [1], Benedicte Yvonne De Winter [1,2], Tom Vanden Berghe [7], Sven Marcel Francque [1,2], Wilhelmus Josephus Kwanten [1,2]

Affiliations:

[1] Laboratory of Experimental Medicine and Pediatrics, Infla-Med Centre of Excellence, University of Antwerp, Antwerp, Belgium

[2] Department of Gastroenterology and Hepatology, Antwerp University Hospital, Antwerp, Belgium

[3] Laboratory of Cell Biology & Histology, Dept. Veterinary Sciences, University of Antwerp, Antwerp, Belgium

[4] Antwerp Centre for Advanced Microscopy (ACAM), University of Antwerp, Antwerp, Belgium

[5] µNEURO Research Excellence Consortium on Multimodal Neuromics, University of Antwerp

[6] Department of Pathology, Antwerp University Hospital, Antwerp, Belgium

[7] Laboratory of Pathophysiology, University of Antwerp, Antwerp, Belgium

* Corresponding author: Cédric Peleman, Laboratory of Experimental Medicine and Pediatrics, University of Antwerp. Universiteitsplein 1, 2610 Antwerpen, Belgium. cedric.peleman@uantwerpen.be, T: +32 3 265 26 32, F: +32 3 265 25 78.

Abstract

Aims: Immunohistochemical stains (IHC) reveal differences between liver lobule zones in health and disease, including non-alcoholic fatty liver disease (NAFLD). However, such differences are difficult to accurately quantify. In NAFLD, the presence of lipid vacuoles from macrovesicular steatosis further hampers interpretation by pathologists. To resolve this, we applied a zonal image analysis method to measure the distribution of hypoxia markers in the liver lobule of steatotic livers.

Methods and results: The hypoxia marker pimonidazole was assessed with IHC in the livers of male C57BL/6J mice on standard diet or choline-deficient L-amino acid-defined high-fat diet mimicking NAFLD. Another hypoxia marker, carbonic anhydrase IX, was evaluated by IHC in human liver tissue. Liver lobules were reconstructed in whole slide images and staining positivity was quantified in different zones in hundreds of liver lobules. This method was able to quantify the physiological oxygen gradient along hepatic sinusoids in normal livers and panlobular spread of the hypoxia in NAFLD, and to overcome the pronounced impact of macrovesicular steatosis on IHC. In a proof-of-concept study with assessment of the parenchyma between centrolobular veins in human liver biopsies carbonic anhydrase IX could be quantified correctly as well.

Conclusions: The method of zonated quantification of IHC objectively quantifies the difference in zonal distribution of hypoxia markers (used as an example) between normal and NAFLD livers both in whole liver as well as in liver biopsy specimens. It constitutes a tool for liver pathologists to support visual interpretation and estimate the impact of steatosis on IHC results.

Keywords

Non-alcoholic fatty liver disease, immunohistochemistry, liver zonation, quantitative evaluation, hypoxia

Introduction

The liver parenchyma is organised into functional zones, wherein hepatocytes and nonparenchymal cell types display different phenotypes depending on their localisation along the liver sinusoids and the circadian rhythm.[1] In various disease states this homeostasis is perturbed, with pathogenic alterations occurring in specific zones or the entirety of the liver lobule. This zonation is widely studied by means of histology and antibody-based detection of biomarkers, but changes are difficult to quantify. For instance, semi-quantitative scoring of immunohistochemistry (IHC) in the centrolobular or periportal zones of the liver lobule can be prone to bias, especially since those zones are not clearly demarcated.[2–5] Quantitative IHC is not yet routine practice in the histopathology field, although efforts are undertaken in digital pathology.[6] The issue of zonal quantification in the liver, however, has not been sufficiently addressed.

Non-alcoholic fatty liver disease (NAFLD), regarded as the hepatic manifestation of the metabolic syndrome, is recognised as a major cause of cirrhosis and second indication for liver transplantation in the US.[7–9] Given its epidemic proportions, affecting roughly a quarter of the global adult population, much (pre)clinical research is conducted to identify druggable targets.[10] NAFLD is defined by presence of vesicles of fat (mainly triglycerides) in the hepatocytes, termed macrovesicular steatosis, which form blank spaces created by hepatocellular lipid vacuoles filling the cytoplasm. Evidently, severe forms of steatosis hamper the interpretation and quantification of the percentage of positively stained area, especially for cytoplasmic markers, as well as comparison with non-steatotic controls.[11] Therefore, we applied a method to zonally quantify the distribution of epitopes within the liver lobule, even in the presence of steatosis, using hypoxia markers as examples in a preclinical model and human liver specimens.

Materials and methods

Animal experiments and Immunohistochemistry

C57BL/6J male mice (Janvier Labs, Le Genest-Saint-Isle, France), housed in 12 hour light-dark cycles and fed ad libitum, were randomised to receive either the choline-deficient L-amino acid defined high-fat diet (CDAHFD, A06071302, Research Diets, New Brunswick, NJ, USA) or standard diet (controls) for three weeks. Subsequently, animals received an intraperitoneal injection of pimonidazole (100mg/kg) one hour prior to sacrifice (n=6 per group). Pimonidazole is a 2-nitroimidazole which is reductively activated in hypoxic cells and forms stable adducts with thiol groups of proteins, peptides and amino acids.[12] Serial sections of formalin-fixed paraffin-embedded (FFPE) liver tissue (5µm thick) were stained with haematoxylin-eosin (H&E) stain, as well as IHC for glutamine synthetase (GS) and pimonidazole adducts (two sets of serial sections per animal). Briefly, heat-induced epitope retrieval was performed with pressure cooker for GS in 0.01M sodium citrate buffer (pH 6.0); endogenous peroxidases and biotin were blocked. Nonspecific binding was blocked with 10% normal goat serum. Primary antibodies for pimonidazole (PAb2627, 1:750, Hypoxyprobe, Burlington, MA, USA) and GS (ab73593, 1:500, Abcam, Cambridge, UK) were incubated overnight at room temperature. Binding of the primary antibody was visualised with VECTASTAIN® ABC-HRP Kit (PK-4001, Vector Laboratories, Newark, CA, USA) and 3,3'-diaminobenzidine (DAB, D8001, Sigma-Aldrich, St. Louis, MO, USA). The ARRIVE guideline for animal pre-clinical studies was used during the preparation of the manuscript.[13]

Human liver specimens and Immunohistochemistry

We studied FFPE human liver tissue obtained from a donor-liver with steatosis, which was rejected because of a high degree of steatosis (>30%). Moreover, percutaneous core needle biopsy material was obtained from three patients referred to the outpatient Hepatology clinic at the Antwerp University Hospital between 2015 and 2019 for mildly elevated transaminase levels. The study was approved by the Ethical Committee of the Antwerp University Hospital (references 6/25/125 and 15/21/227) and patients gave written consent for the collection of material. Serial sections of liver tissue (5µm thick)

were stained with IHC for GS (ab73593, 1:500, Abcam, UK) and carbonic anhydrase IX (CAIX, PA1-16592, Invitrogen, US) as described above.

Whole slide imaging acquisition and data processing

Slides from all murine and human liver specimens were digitalised using the Zeiss Axioscan Z1 automated whole slide scanner (Zeiss, Germany) using a 20x objective lens (pixel size 0,22 x 0,22 µm). A whole slide image was loaded into FIJI image processing freeware and subjected to the image analysis script described in supplemental materials.[14] Briefly, colour deconvolution was applied on pimonidazole IHC to isolate the DAB signal which was binarised by means of the Percentile autothreshold algorithm to identify positively stained area.[15, 16] A separate segmentation based on manual thresholding (grey values of 190 and above) and subsequent size (53-580µm) and circularity (0.5-1.00) filtering was performed to annotate the majority of lipid vacuoles.[17] These parameters for lipid vacuole detection minimise false-positive selections (only clear macrovesicular steatosis), while accepting more false-negatives, and were applied uniformly on all images to avoid operator-dependent bias. Liver lobules are organised according to a principle that is best described by Voronoi diagrams.[5, 18] Hence, we implemented a routine that delineates all lobules by means of Voronoi tessellation after manual annotation of central veins, based on morphology on H&E and IHC for GS, and the liver capsule. GS is a well-known marker of hepatocytes adjacent to the centrolobular vein.[19] Next, pixels within each lobule were assigned with a relative distance value (0 at the lobular edge to 1 in the centrolobular vein) and visualised with a corresponding colour for each relative distance using the look-up table '16 colors'. The results were processed in RStudio, expanded with the R-package "dplyr" for grouped summary statistics to produce heatmaps and calculate the zonation of pimonidazole positivity.[20]

'Digital' biopsies of a preclinical NAFLD model

In clinical practice, there is more availability of needle biopsy material but reconstruction of whole liver lobules is difficult due to the small amount of liver tissue in that setting, the limited number of centrolobular veins and the absence of the liver capsule in the biopsy specimen. The method of zonated quantification of IHC was hence adapted for use in needle biopsy specimens. Indeed, the relative

distance can be correctly assessed in parenchyma directly connecting different centrolobular veins, so-called centro-central tracts, which are available in needle biopsy specimens. Based on the anatomy of the Kiernan's lobule the portal area will be situated between the centrolobular veins in the middle of the centro-central tracts. We tested this approach by performing 'digital' liver biopsies in the murine liver slides analysed above, in order to compare the analysis in whole liver slides with the centro-central approach. Random 'digital' biopsies (rectangular areas of 300µm x 50µm in size, equivalent to a small liver biopsy) were hence selected from whole liver slides of C57BL/6J male mice fed CDAHFD or standard diet (controls) and analysed isolatedly. These specimens of liver tissue contained 3 to 5 centrolobular veins to reconstruct the relative distance maps.

Statistical analyses

Proportions of pimonidazole positive areas and ratios thereof in periportal vs. centrolobular zones from all laboratory mice were expressed as mean±standard deviation. Differences between normal and diseased subjects were assessed for statistical significance with the Mann-Whitney U test. Means of periportal vs. centrolobular ratio assessed in whole liver slides and centro-central tracts were compared by paired T-test. Intraclass correlation coefficients (ICC) for absolute agreement were calculated to examine agreement between the two methods of zonated quantification of hypoxia marker pimonidazole obtained from analysis of whole liver slides and the 'digital' liver biopsies in the same experimental subjects. ICC values were interpreted as follows: 0-0.2 corresponds to poor agreement, 0.3-0.4 corresponds to fair agreement, 0.5-0.6 corresponds to moderate agreement, 0.7-0.8 corresponds to strong agreement, and >0.8 indicates near perfect agreement.[21] Statistical analysis was performed with SPSS (version28; IBM, USA). All figures were generated using GraphPad Prism (version 9.0; GraphPad Software, USA).

Results

Histology of a preclinical NAFLD model and IHC for pimonidazole adducts shows panlobular hypoxia in NASH

After three weeks all mice on CDAHFD displayed the features of non-alcoholic steatohepatitis (NASH), as opposed to the controls.[22] In healthy livers, the physiological oxygen gradient was demonstrated by corresponding pimonidazole adducts with positivity in the centrolobular area attenuating towards the periportal triads (Fig. 1A upper panel).[23] However, in NASH the staining for pimonidazole adducts was more equally present throughout the whole liver lobule but interrupted by lipid vacuoles, in agreement with other reports (Fig. 1A upper panel).[24, 25] It is known that steatosis in this model is more pronounced in the periportal zones (Fig. 1A middle panel).[22] GS expression was limited to hepatocytes around the centrolobular veins, both in normal and NASH livers (Fig. 1A lower panel). The DAB signal of pimonidazole IHC was presented as a heatmap to demonstrate widespread intense positive staining of the liver parenchyma in CDAHFD compared to more focal positivity around centrilobular veins in controls (Fig. 1B upper panel). Of note, no staining signal was detected upon omission of the primary antibody directed against pimonidazole adducts (Fig. S1). Subsequently, centrolobular veins served as seeds for liver lobule reconstructions and pixels within each lobule received a relative distance value ranging from 0 (at the lobular edge) to 1 (in the centrolobular vein). This relative distance map is illustrated by the lower panel of Fig. 1B, wherein each colour represents points with the same relative distance between centre (centrolobular veins annotated in white) and edge (annotated in black) of each constructed lobule.

Zonated quantification of immunohistochemistry confirms the periportal increase in pimonidazole positivity in a preclinical NASH model vs normal livers

Next, the pimonidazole positive area occupancy (area %) and macrovesicular steatotic area occupancy (area %) were quantified as a function of the relative distance within individual liver lobules of all laboratory mice included in this study (Figures 2A and 2B). The amount of pimonidazole positive area

is diluted by the presence of macrovesicular steatosis (which itself is not uniformly distributed) since lipid vacuoles occupy space. However, when these lipid vacuoles were excluded from the analysis, the amount of pimonidazole positive area was significantly higher in the periportal zone of the lobules from mice on CDAHFD compared to controls ($p<0.01$; Fig. 2C).

Moreover, to express the zonal distribution in a single value, the ratio of pimonidazole positive areas in periportal vs. centrolobular thirds of all lobules was calculated without exclusion of lipid vacuoles. This ratio was low in healthy livers, thereby reflecting the physiological hypoxia towards the centre of Kiernan's liver lobule, but was significantly higher in NASH livers in accordance with panlobular positivity ($p<0.001$; Fig. 2D).

'Digital' biopsies of a preclinical NAFLD model

Analysis of 'digital' biopsies of all laboratory mice of the preclinical NAFLD model revealed significant periportal pimonidazole positivity in centro-central tracts of NASH livers compared to controls, after exclusion of lipid vacuoles (Fig. 3A-C). Therefore, the analysis of the liver parenchyma between centrolobular veins detected similar trends as whole liver slides. The means of periportal vs. centrolobular ratios differed significantly between the two methods ($p = 0.004$ when including lipid droplets, $p = 0.003$ when excluding lipid droplets), indicating the presence of a systematic difference with higher ratios in the centro-central approach compared to whole liver slides (Fig. S2). In other words, the lobular gradient of pimonidazole positivity is less steep when analysing the centro-central tracts, partly due to higher periportal pimonidazole positive area, compared to whole liver slides. In addition, the ICC between the two methods showed moderate to strong agreement for IHC for pimonidazole in the preclinical NAFLD model: ICC absolute agreement 0.823 (95% CI 0.486-0.930, $p<0.001$) when including lipid droplets, ICC absolute agreement 0.866 (95% CI 0.568-0.949, $p<0.001$) when excluding lipid droplets.

Application of zonated quantification of immunohistochemistry in human liver material

An area of a liver resection specimen with steatosis was assessed with IHC for CAIX (Fig. 4A). This hypoxia marker displayed foci of strong positivity in the centrolobular area (Fig. 4B). As proof of concept, liver lobules were reconstructed (Fig. 4C) and IHC for CAIX was quantified in different zones (Fig. 4D), thereby confirming the centrolobular nature of this epitope through accurate, objective quantification of the staining pattern.

Finally, in order to further test the centro-central approach in humans, three human needle biopsy specimens were stained with IHC and revealed panlobular, intense positivity for CAIX in two NASH subjects, compared to one control (Fig. 5A upper panels). Next, distance maps were reconstructed between centrolobular veins (Fig. 5A lower panels) and the staining pattern of CAIX was plotted in these centro-central tracts (Fig. 5B). The distribution of CAIX was even in different zones of the liver lobule with a higher proportion of positive area in the NASH patients compared to control. Fig S3 displays the whole slide images of the three needle biopsy specimens.

Discussion

The method described in this manuscript quantifies the location of IHC stains within the liver lobule in normal and steatotic livers, using hypoxia markers as examples. After reconstruction of lobules IHC staining patterns are quantified according to the relative distance. Interpretation by pathologists is of paramount relevance, but accurate quantification supports conclusions. Moreover, instead of showing only representative images or analysing 'random' fields per tissue slide which can introduce observer bias, this method analyses and represents a staining pattern of hundreds of lobules in an objective way. The exclusion of areas occupied by lipid droplets enhanced the interpretation of the zonal staining patterns, compared with the whole liver slide area containing lipid vacuoles which are by their nature unable to stain positively. It enables the pathologist to better assess the (zonal) impact of steatosis on IHC results. In addition, 'digital' biopsies drawn from mice livers demonstrate moderate-to-strong agreement between whole liver analysis for pimonidazole compared to more limited liver tissue. The 'digital' biopsies represent only a small part of the liver tissue and increasing the size/length or number of those samples could further enhance the agreement with whole liver analysis. Subsequent proof-of-concept in a human surgical resection specimen and needle biopsy specimens another hypoxia marker suggests that this method could also be used in the human, clinical pathology setting. This can be further explored in large cohorts of human needle biopsy specimens stained with IHC for various epitopes. Importantly, in this study steatotic livers and hypoxia markers serve to demonstrate this objective zonal IHC quantification, which could be applied to various epitopes in normal livers and multiple hepatologic diseases.

Within the healthy liver lobule hepatocytes differentiate to perform very different enzymatic and metabolic functions depending on their position along the sinusoid. For example, periportal hepatocytes perform gluconeogenesis, oxidation of fatty acids and ammonia detoxification, whereas their perivenous counterparts express enzymes required for glycolysis, lipogenesis and drug metabolism. Detailed single-cell spatial reconstruction revealed that functional separation into nine layers of hepatocytes could be more accurate than the traditional three lobular zones.[26] Regulators of the phenomenon of zonation are the gradients of oxygen, nutrients, hormones, as well as various molecular pathways (*e.g.* Wnt/β-

catenin, hedgehog), but knowledge of these regulators is incomplete.[19, 27] Functional organisation of the liver lobule is perturbed in pathologic conditions with nearly every disease entity displaying a distinct topography. Histological abnormalities in NAFLD, for instance, mostly start in the centrolobular area, which is also severely affected in ischemic hepatitis and drug-induced liver injury.[19, 28] Conversely, the inflammatory infiltrate of auto-immune hepatitis radiates from the portal triads to infiltrate the parenchyma.[29] Topography of histological abnormalities and IHC stains supports pathologists to make the correct diagnosis (or combinations thereof) in individual patients. The proposed method could accurately describe the location and extent of histological abnormalities and evolution within disease progression/regression in routine practice after validation.

Moreover, the method of zonated quantification of IHC could be applied more readily in the setting of clinical trials and translational research. IHC stains typically provide qualitative data and descriptions, which semi-quantitative scoring can transform into data amenable to statistical analysis in the setting of research, through separation into ordinal classes.[30] However, semi-quantitative scoring has limitations since it relies on labour-intensive, manual observations susceptible to some levels of observer variability.[3, 4] For instance, the H-score combines the percentage of HER2 positive cells and their stain intensity, visually estimated by the pathologist, to guide treatment decisions.[31] The results of this subjecting scoring are influenced by histological expertise and agreement could be improved by computer-aided digital microscopy.[32, 33] Moreover, the human visual system has limited ability to detect subtle differences, especially in the low intensity range.[34, 35] Hence, image analysis systems that yield continuous data, such as the zonated quantification method presented above, may assist pathologists and researchers in detecting subtle differences.

Indeed, the field of digital pathology has enjoyed much interest in the last decade of (pre)clinical liver research both autonomous and in conjunction with classical pathology reading. Most of the research effort has focused on artificial intelligence imaging for automated detection and quantification of histological hallmarks of disease, *i.e.* macrovesicular steatosis, ballooning, lobular inflammation and fibrosis in NAFLD.[6, 36–39] Various machine learning algorithms based on deep convolutional networks are trained to count those features. For instance, Naoumov *et al.* recently demonstrated that

reanalysis of human liver biopsies with artificial intelligence revealed an antifibrotic effect of tropifexor that was not evidenced by conventional scoring.[40] Hence, these systems might allow for a more granular assessment of (drug-induced) changes in histological features. Of note, compared to degree of positive area, semi-quantitative scoring of liver biopsy remains more reliant on the training sets based on annotation by multiple human pathologists.[37, 41] However, to the best of our knowledge, accurate evaluation of zonation within the liver lobule of those key histological features has not been incorporated in the existing systems. The method presented herein could be enhanced with automated detection of centrolobular veins to allow for higher throughput. Next, the aspect of liver zonation could be added to digital pathology to describe in more detail the distribution of key histological hallmarks and different epitopes assessed with IHC. Alternative methods to assess zonation would be (rather cumbersome) manual counting of positive hepatocytes in rows radiating outwards from the central veins or subjective estimation of the centrolobular or periportal zones.[2, 42] The latter is less accurate given that the lobular zones are not visibly anatomically delineated.

Furthermore, in this study we chose to quantify the percentage of IHC positive area in relation to the lobular regions. Alternatively, machine learning and pixel classifiers could have counted the percentage of positive hepatocytes to use a cell-based quantification instead of the pixel-based approach. Cell-based automated detection has been employed for quantification of hypoxia markers in other cell types and can differentiate between nuclear and cytoplasmic positivity.[43, 44] However, such cell-based recognition might be challenging in steatosis given the abundance of lipid vacuoles which are actually hepatocytes without stainable cytoplasm and whose nuclei can be situated outside the sectioning plane.[45] Nevertheless, cell-based and pixel-based methods of quantification could be mutually supportive.

A limitation of the method presented herein is that compound lobules, tangential sectioning of lobules and tears in whole liver tissue slides can reduce accurate reconstruction of liver lobules. These limitations are intrinsic to the 2D representation of 3D structures and could be partially resolved by whole liver serial sectioning and 3D reconstruction of lobules. Validation of this method for the detection of zonation of other epitopes is needed. Moreover, the CDAHFD dietary model induces

histological abnormalities of NASH but lacks other features of the metabolic syndrome, such as visceral adiposity and systemic insulin resistance.[22] Indeed, the pathophysiology of NAFLD is very complex with intrahepatic alterations, such as vascular alterations, lipotoxicity, cell death, immune cell infiltration and important cellular matrix alterations with liver fibrosis, which are intricately related to the systemic alterations of the metabolic syndrome.[46–50] Choline-deficient diets, such as the CDAHFD, are considered and accepted liver-centred models with pronounced steatosis to exemplify the method of zonated IHC quantification.[51] The pattern of liver fibrosis was not a subject in the present study. In addition, the use of the proposed method in other liver diseases, *e.g.* alcohol related liver disease and chronic hepatitis C which can also bear macrovesicular steatosis as a hallmark, is worthwhile to investigate. Moreover, in this study we used the avidin-biotin complex (ABC) system to visualise epitopes, whereas a two-step method based on a horse radish peroxidase (HRP) labelled polymer conjugated with secondary antibodies (*e.g.* EnVision+ system) is increasingly used. This highly sensitive assay avoid interference from endogenous biotin, but comes at greater cost per unit of detection system.[52] In our study endogenous biotin was blocked and a negative control for the ABC detection system excluded false positivity due to any remaining endogenous biotin. The quantification method for DAB positivity could be applied for both HRP-based detection systems. Finally, the strength is the use of a simple algorithm combining previously described open-source methods that is manageable by non-experts in advanced image processing.

In conclusion, this method enables objective zonal quantification of IHC for hypoxia marker pimonidazole in liver in a preclinical model, even when severely steatotic, and can improve interpretation of the marker of interest. We provide proof-of-concept that this method could also be applied to human needle biopsies, paving the way for its use in the clinical pathology setting.

Acknowledgements

We thank Sofie Thys for technical assistance with scanning of the slides. This study was funded by the Fund for Scientific Research (FWO) Flanders (1171121N), research grants of the University of Antwerp (GOA project: FFB180348/36572) and the Belgian Association for the Study of the Liver (BASL basic research award 2020 supported by Gilead).

Abbreviations

ABC, avidin-biotin complex; CAIX, carbonic anhydrase IX; CDAHFD, choline-deficient L-amino acid-defined high-fat diet; CL, centrolobular; DAB, 3,3'-diaminobenzidine; FFPE, formalin-fixed paraffin-embedded; GS, glutamine synthetase; H&E, haematoxylin-eosin; HRP, horse radish peroxidase; ICC, intraclass correlation coefficient; IHC, immunohistochemistry; NAFLD, non-alcoholic fatty liver disease; NASH, non-alcoholic steatohepatitis; Pimo, pimonidazole; PP, periportal

List of online Supporting Information

Plugin for FIJI, title: Zonated_portality_measurement.ijm. Also available at: https://github.com/DeVosLab/Steatosis_ZonatedPortality

Supplementary Figure S1. Comparison of ratio of periportal vs. centrolobular Pimonidazole positive area assessed in whole liver slides and centro-central tracts in a preclinical NAFLD model.

Supplementary Figure S2. Whole slide liver images of IHC on human needle biopsy specimens.

Statements and Declarations

Data Availability Statement: The whole slide image data used to support the findings of this study are available from the corresponding author at cedric.peleman@uantwerpen.be upon request.

Funding: C.P. received funding from the Fund for Scientific Research (FWO) Flanders (1171121N). This study was funded by research grants of the University of Antwerp (GOA project: FFB180348/36572) and the Belgian Association for the Study of the Liver (BASL basic research award 2020 supported by Gilead). The funders had no role in study design, collection, analysis or interpretation of data, or writing of the report.

Conflict of interest disclosure: All authors declare that they have no financial or non-financial interests related to this manuscript.

Ethics Approval and Consent to Participate: All animal experiment presented in this work were approved by the Ethical Committee of Animal Experimentation of the University of Antwerp (Protocol number: 2019-42). All animals received humane care in accordance with the "Guide for the Care and Use of Laboratory Animals (Eighth Edition)" prepared by the National Academy of Sciences and published by the National Institutes of Health. Human data reported in this study was obtained from patients who gave written consent for the collection of material; the protocols were conformed to the ethical guidelines of the latest version of the Declaration of Helsinki. The study was approved by the Ethical Committee of the Antwerp University Hospital (references 6/25/125 and 15/21/227).

Authors' contributions: C.P., W.H.D., T.V., W.J.K. conceptualization and design of research; C.P., J.D., A.V. performed experiments; C.P., W.H.D. software and formal analysis; C.P. drafted manuscript and prepared figures; I.P. methodology; W.H.D., I.P., A.D., A.V., C.V., L.V., J.D., B.D., T.V. S.M.F. and W.J.K. edited and revised manuscript; C.P., W.H.D., I.P., A.D., A.V., C.V., L.V., J.D., B.D., T.V., S.M.F. and W.J.K. seen and approved final version of manuscript.

References

1. Droin C, Kholtei J El, Bahar Halpern K, et al (2021) Space-time logic of liver gene expression at sub-lobular scale. Nat Metab 3:43–58. https://doi.org/10.1038/s42255-020-00323-1

2. Seki S, Kitada T, Yamada T, et al (2002) In situ detection of lipid peroxidation and oxidative DNA damage in non-alcoholic fatty liver diseases. J Hepatol 37:56–62. https://doi.org/10.1016/S0168-8278(02)00073-9

3. Meyerholz DK, Beck AP (2018) Principles and approaches for reproducible scoring of tissue stains in research. Lab Investig 98:844–855. https://doi.org/10.1038/s41374-018-0057-0

4. Walker RA (2006) Quantification of immunohistochemistry - Issues concerning methods, utility and semiquantitative assessment I. Histopathology 49:406–410. https://doi.org/10.1111/j.1365-2559.2006.02514.x

5. Lau C, Kalantari B, Batts KP, et al (2021) The Voronoi theory of the normal liver lobular architecture and its applicability in hepatic zonation. Sci Rep 11:9343. https://doi.org/10.1038/s41598-021-88699-2

6. Taylor-Weiner A, Pokkalla H, Han L, et al (2021) A Machine Learning Approach Enables Quantitative Measurement of Liver Histology and Disease Monitoring in NASH. Hepatology 74:133–147. https://doi.org/10.1002/hep.31750

7. Setiawan VW, Stram DO, Porcel J, et al (2016) Prevalence of chronic liver disease and cirrhosis by underlying cause in understudied ethnic groups: The multiethnic cohort. Hepatology 64:1969–1977. https://doi.org/10.1002/hep.28677

8. Goldberg D, Ditah IC, Saeian K, et al (2017) Changes in the Prevalence of Hepatitis C Virus Infection, Nonalcoholic Steatohepatitis, and Alcoholic Liver Disease Among Patients With Cirrhosis or Liver Failure on the Waitlist for Liver Transplantation. Gastroenterology 152:1090–1099. https://doi.org/10.1053/j.gastro.2017.01.003

9. Wong RJ, Aguilar M, Cheung R, et al (2015) Nonalcoholic steatohepatitis is the second leading

etiology of liver disease among adults awaiting liver transplantation in the United States. Gastroenterology 148:547–555. https://doi.org/10.1053/j.gastro.2014.11.039

10. Younossi ZM, Koenig AB, Abdelatif D, et al (2016) Global epidemiology of nonalcoholic fatty liver disease—Meta-analytic assessment of prevalence, incidence, and outcomes. Hepatology 64:73–84. https://doi.org/10.1002/hep.28431

11. Ghallab A, Myllys M, Friebel A, et al (2021) Spatio-temporal multiscale analysis of western diet-fed mice reveals a translationally relevant sequence of events during NAFLD progression. Cells 10:2516. https://doi.org/10.3390/cells10102516

12. Raleigh JA, Koch CJ (1990) Importance of thiols in the reductive binding of 2-nitroimidazoles to macromolecules. Biochem Pharmacol 40:2457–2464. https://doi.org/10.1016/0006-2952(90)90086-Z

13. Percie N, Hurst V, Ahluwalia A, et al (2020) The ARRIVE guidelines 2.0: updated guidelines for reporting animal research. BMJ Open Sci 1–7. https://doi.org/10.1136/bmjos-2020-100115

14. Schindelin J, Arganda-Carreras I, Frise E, et al (2012) Fiji: An open-source platform for biological-image analysis. Nat Methods 9:676–682. https://doi.org/10.1038/nmeth.2019

15. Ruifrok AC, Johnston DA (2001) Quantification of histochemical staining by color deconvolution. Anal Quant Cytol Histol 23, 291–299 10–27

16. Doyle W (1962) Operations Useful for Similarity-Invariant Pattern Recognition. J ACM 9:259–267. https://doi.org/10.1145/321119.321123

17. Munsterman ID, van Erp M, Weijers G, et al (2019) A Novel Automatic Digital Algorithm that Accurately Quantifies Steatosis in NAFLD on Histopathological Whole-Slide Images. Cytom Part B 96:521–528. https://doi.org/10.1002/cyto.b.21790

18. Schwen LO, Homeyer A, Schwier M, et al (2016) Zonated quantification of steatosis in an entire mouse liver. Comput Biol Med 73:108–118. https://doi.org/10.1016/j.compbiomed.2016.04.004

19. Panday R, Monckton CP, Khetani SR (2022) The Role of Liver Zonation in Physiology, Regeneration, and Disease. Semin Liver Dis 42:1–16. https://doi.org/10.1055/s-0041-1742279

20. R Core Team (2018) R: A Language and Environment for Statistical Computinng. In: R Found. Stat. Comput. Vienna. https://www.r-project.org

21. Landis JR, Koch GG (1977) The Measurement of Observer Agreement for Categorical Data. Biometrics 33:159–174. https://doi.org/10.2307/2529310

22. Matsumoto M, Hada N, Sakamaki Y, et al (2013) An improved mouse model that rapidly develops fibrosis in non-alcoholic steatohepatitis. Int J Exp Pathol 94:93–103. https://doi.org/10.1111/iep.12008

23. Kietzmann T (2019) Liver zonation in health and disease: Hypoxia and hypoxia-inducible transcription factors as concert masters. Int J Mol Sci 20:2347. https://doi.org/10.3390/ijms20092347

24. Mantena SK, Vaughn DP, Andringa KK, et al (2009) High fat diet induces dysregulation of hepatic oxygen gradients and mitochondrial function in vivo. Biochem J 417:183–193. https://doi.org/10.1042/BJ20080868

25. Meng L, Goto M, Tanaka H, et al (2021) Decreased Portal Circulation Augments Fibrosis and Ductular Reaction in Nonalcoholic Fatty Liver Disease in Mice. Am J Pathol 191:1580–1591. https://doi.org/10.1016/j.ajpath.2021.06.001

26. Ben-Moshe S, Shapira Y, Moor AE, et al (2019) Spatial sorting enables comprehensive characterization of liver zonation. Nat Metab 1:899–911. https://doi.org/10.1038/s42255-019-0109-9

27. Paris J, Henderson NC (2022) Liver zonation, revisited. Hepatology 76:1219–1230. https://doi.org/10.1002/hep.32408

28. Cunningham RP, Porat-Shliom N (2021) Liver Zonation – Revisiting Old Questions With New Technologies. Front Physiol 12:1–17. https://doi.org/10.3389/fphys.2021.732929

29. Czaja AJ, Carpenter HA (1993) Sensitivity, specificity, and predictability of biopsy interpretations in chronic hepatitis. Gastroenterology 105:1824–1832. https://doi.org/10.1016/0016-5085(93)91081-R

30. Meyerholz DK, Beck AP (2018) Fundamental Concepts for Semiquantitative Tissue Scoring in Translational Research. ILAR J 59:13–17. https://doi.org/10.1093/ilar/ily025

31. McCarty K, Szabo E, Flowers J, et al (1986) Use of a monoclonal anti-estrogen receptor antibody in the immunohistochemical evaluation of human tumors. Cancer Res 46:4244–4248

32. Gavrielides MA, Gallas BD, Lenz P, et al (2011) Observer variability in the interpretation of HER2/neu immunohistochemical expression with unaided and computer-aided digital microscopy. Arch Pathol Lab Med 135:233–242. https://doi.org/10.5858/135.2.233

33. Skaland I, Øvestad I, Janssen EAM, et al (2008) Digital image analysis improves the quality of subjective HER-2 expression scoring in breast cancer. Appl Immunohistochem Mol Morphol 16:185–190. https://doi.org/10.1097/PAI.0b013e318059c20c

34. Rimm DL, Giltnane JM, Moeder C, et al (2007) Bimodal population or pathologist artifact? [1]. J Clin Oncol 25:2487–2488. https://doi.org/10.1200/JCO.2006.07.7537

35. Camp RL, Dolled-Filhart M, King BL, Rimm DL (2003) Quantitative analysis of breast cancer tissue microarrays shows that both high and normal levels of HER2 expression are associated with poor outcome. Cancer Res 63:1445–1448

36. Liu F, Goh GBB, Tiniakos D, et al (2020) qFIBS: An Automated Technique for Quantitative Evaluation of Fibrosis, Inflammation, Ballooning, and Steatosis in Patients With Nonalcoholic Steatohepatitis. Hepatology 71:1953–1966. https://doi.org/10.1002/hep.30986

37. Brunt EM, Clouston AD, Goodman Z, et al (2022) Complexity of ballooned hepatocyte feature recognition: Defining a training atlas for artificial intelligence-based imaging in NAFLD. J Hepatol 76:1030–1041. https://doi.org/10.1016/j.jhep.2022.01.011

38. Forlano R, Mullish BH, Giannakeas N, et al (2020) High-Throughput, Machine Learning–

Based Quantification of Steatosis, Inflammation, Ballooning, and Fibrosis in Biopsies From Patients With Nonalcoholic Fatty Liver Disease. Clin Gastroenterol Hepatol 18:2081–2090. https://doi.org/10.1016/j.cgh.2019.12.025

39. Bosch J, Chung C, Carrasco-Zevallos OM, et al (2021) A Machine Learning Approach to Liver Histological Evaluation Predicts Clinically Significant Portal Hypertension in NASH Cirrhosis. Hepatology 74:3146–3160. https://doi.org/10.1002/hep.32087

40. Naoumov N V., Brees D, Loeffler J, et al (2022) Digital pathology with artificial intelligence analyses provides greater insights into treatment-induced fibrosis regression in NASH. J Hepatol DOI: 10.1016/j.jhep.2022.06.018. https://doi.org/10.1016/j.jhep.2022.06.018

41. Davison BA, Harrison SA, Cotter G, et al (2020) Suboptimal reliability of liver biopsy evaluation has implications for randomized clinical trials. J Hepatol 73:1322–1332. https://doi.org/10.1016/j.jhep.2020.06.025

42. Arteel GE, Iimuro Y, Yin M, et al (1997) Chronic enteral ethanol treatment causes hypoxia in rat liver tissue in vivo. Hepatology 25:920–926. https://doi.org/10.1002/hep.510250422

43. Zaidi M, Fu F, Cojocari D, et al (2019) Quantitative Visualization of Hypoxia and Proliferation Gradients Within Histological Tissue Sections. Front Bioeng Biotechnol 7:1–9. https://doi.org/10.3389/fbioe.2019.00397

44. Swartz JE, Smits HJG, Philippens MEP, et al (2022) Correlation and colocalization of HIF-1α and pimonidazole staining for hypoxia in laryngeal squamous cell carcinomas: A digital, single-cell-based analysis. Oral Oncol 128:105862. https://doi.org/10.1016/j.oraloncology.2022.105862

45. Podszun MC, Chung JY, Ylaya K, et al (2020) 4-HNE Immunohistochemistry and Image Analysis for Detection of Lipid Peroxidation in Human Liver Samples Using Vitamin E Treatment in NAFLD as a Proof of Concept. J Histochem Cytochem 68:635–643. https://doi.org/10.1369/0022155420946402

46. Francque S, Verrijken A, Mertens I, et al (2010) Noncirrhotic human nonalcoholic fatty liver disease induces portal hypertension in relation to the histological degree of steatosis. Eur J Gastroenterol Hepatol 22:1449–1457. https://doi.org/10.1097/MEG.0b013e32833f14a1

47. Parthasarathy G, Revelo X, Malhi H (2020) Pathogenesis of Nonalcoholic Steatohepatitis: An Overview. Hepatol Commun 4:478–492. https://doi.org/10.1002/hep4.1479

48. Peiseler M, Schwabe R, Hampe J, et al (2022) Immune mechanisms linking metabolic injury to inflammation and fibrosis in fatty liver disease – novel insights into cellular communication circuits. J Hepatol 77:1136–1160. https://doi.org/10.1016/j.jhep.2022.06.012

49. Doi Y, Tamura S, Nammo T, et al (2007) Development of complementary expression patterns of E- and N-cadherin in the mouse liver. Hepatol Res 37:230–237. https://doi.org/10.1111/j.1872-034X.2007.00028.x

50. Kisseleva T, Brenner D (2021) Molecular and cellular mechanisms of liver fibrosis and its regression. Nat Rev Gastroenterol Hepatol 18:151–166. https://doi.org/10.1038/s41575-020-00372-7

51. Machado MV, Michelotti GA, Xie G, et al (2015) Mouse models of diet-induced nonalcoholic steatohepatitis reproduce the heterogeneity of the human disease. PLoS One 10:1–16. https://doi.org/10.1371/journal.pone.0127991

52. Sabattini E, Bisgaard K, Ascani S, et al (1998) The EnVision(TM)+ system: A new immunohistochemical method for diagnostics and research. Critical comparison with the APAAP, ChemMate(TM), CSA, LABC, and SABC techniques. J Clin Pathol 51:506–511. https://doi.org/10.1136/jcp.51.7.506

Figure legends

Figure 1. Representative pictures of immunohistochemistry (IHC) and reconstructed liver lobules in C57BL/6J mice fed the choline-deficient L-amino acid-defined high-fat diet (CDAHFD) or standard diet (control) for three weeks. (A) Representative images of IHC for pimonidazole adducts (Pimo) and glutamine synthetase (GS), and lipid vacuoles from macrovesicular steatosis (annotated in blue). Pimonidazole is present around centrolobular veins in controls but displays panlobular distribution in CDAHFD. The enzyme GS is expressed in centrolobular hepatocytes. (B) The upper panel shows representative images of deconvoluted DAB signal for Pimo adducts, presented with the pseudocolour image 'Red Hot'. Next, the lower panel displays reconstructed lobules in whole slide liver images with centrolobular veins displayed in white. Each pixel in the whole liver slide received a value ranging from 0 (edge of lobule) to 1 (the centrolobular vein) which represents its relative distance within the constructed liver lobule. Each colour of the look-up table '16 colors' shows points at the same relative distance between the centre and lobular edge (annotated in black) within these lobules.

Figure 2. Zonated quantification of Pimonidazole immunohistochemistry in a mouse model of non-alcoholic steatohepatitis (NASH) vs. normal livers. (A) The percentage of Pimo positive area is calculated at eleven points of relative distance from centre to edge within each lobule on the x-axis. The graph represents the trend in Pimo IHC along the sinusoid in over 700 liver lobules from all laboratory animals included in this study (NASH vs controls) (n=6). (B) Y-axis in this graph represents the proportion of surface occupied by macrovesicular steatosis, as annotated in Fig. 1A middle panel. (C) After exclusion of lipid vacuoles, the percentage of pimonidazole positive area is significantly higher in the periportal zone in CDAHFD compared to controls. (D) The ratio of pimonidazole positive area in periportal (PP) vs. centrolobular (CL) regions is compared in healthy and NASH subjects. Results are presented as mean ± standard deviation. Mann-Whitney U test; **p<0.01, ***p<0.001. Scale bar represents 200µm or 1000µm.

Figure 3. Zonated quantification of immunohistochemistry (IHC) in centro-central tracts of 'digital' liver biopsies in C57BL/6J mice fed the choline-deficient L-amino acid-defined high-fat diet (CDAHFD) or standard diet (control) for three weeks. (A) Representative images of a 'digital'

biopsy in control liver stained with IHC for pimonidazole adducts (Pimo). Relative distances within lobules were reconstructed in the digital biopsy and the staining pattern of Pimo was assessed in the parenchyma directly connecting different centrolobular veins, termed centro-central tracts (black rectangles). (B) Y-axis in this graph represents the proportion of Pimo positive area in centro-central tracts of digital liver biopsies from NASH and controls (n=12). The latter display centrolobular positivity for this hypoxia marker. (C) After exclusion of lipid vacuoles, the percentage of pimonidazole positive area is significantly higher in the periportal zone in CDAHFD compared to controls ($p<0.05$). Hence, the quantification in centro-central tracts detected the same trends as evaluation in whole liver slides (Fig. 2). Results are presented as mean ± standard deviation. Mann-Whitney U test; *$p<0.05$. Scale bar represents ~~1~~200µm.

Figure 4. Quantification of immunohistochemistry for carbonic anhydrase IX in human liver resection specimen with steatosis. (A) Immunohistochemistry for carbonic anhydrase IX (CAIX) revealed foci of strong positivity in a human resection specimen with steatosis. (B) Subjective evaluation of the inset of this image reveals that positivity for CAIX is mainly located near centrolobular veins in this specimen. (C) Annotated centrolobular veins (white dots) acted as references to reconstruct whole liver lobules. Of note, lobules near the edge of the specimen where excluded from further analysis, since the relative distance is less reliable there. (D) The positivity for CAIX (on y-axis) was plotted against the relative distance in liver lobules (on x-axis). The curve visualises the zonal distribution of hypoxia marker CAIX in this liver resection specimen. Scale bar represents 5mm or 200µm.

Figure 5. Proof-of-concept: study of the staining pattern of carbonic anhydrase IX in centro-central tracts in human percutaneous liver biopsies with nonalcoholic steatohepatitis (NASH) or control. (A) Immunohistochemistry for carbonic anhydrase IX (CAIX) revealed more intense positivity in all lobular zones in percutaneous liver biopsy material of two NASH patients (NASH1 and NASH2) compared to control (upper panel). Next, we constructed the relative distance in the parenchyma spanning between centrolobular veins, termed the centro-central tracts (lower panel). (B) Zonal quantification of CAIX positivity in those centro-central tracts confirmed increased positivity of the hypoxia marker in specimens with NASH, compared to control, and illustrates differences between

NASH patients. After exclusion of lipid vacuoles from analysis, the curves of NASH specimens shift slightly upward (dashed lines). Scale bar represents 10µm or 20µm.

Figures

Figure 1.

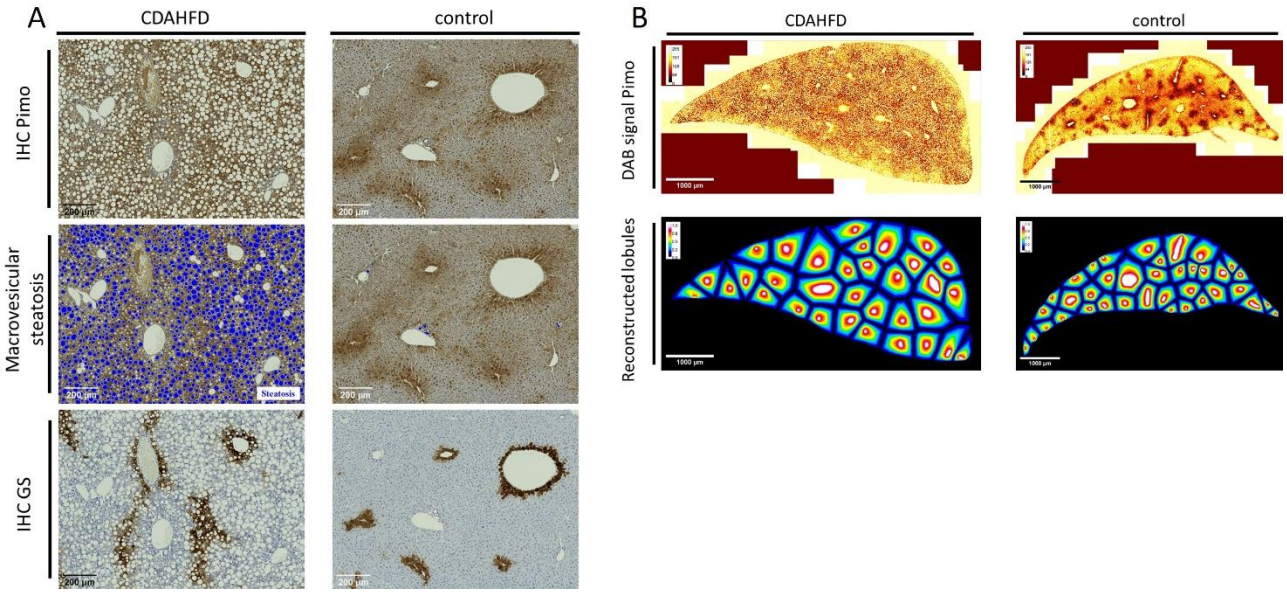

Figure 2.

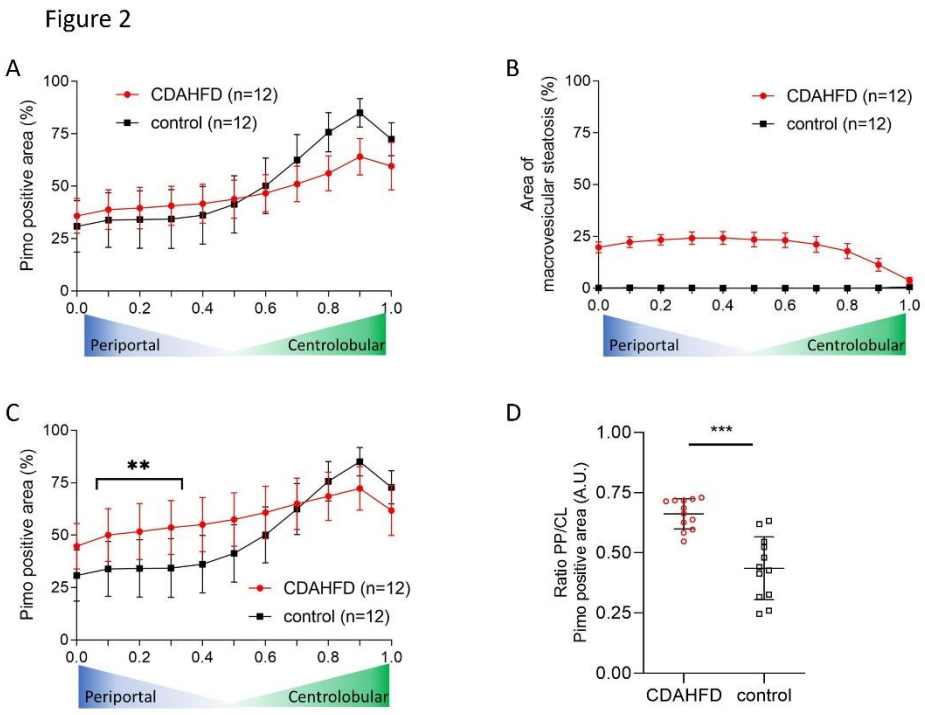

Figure 3.

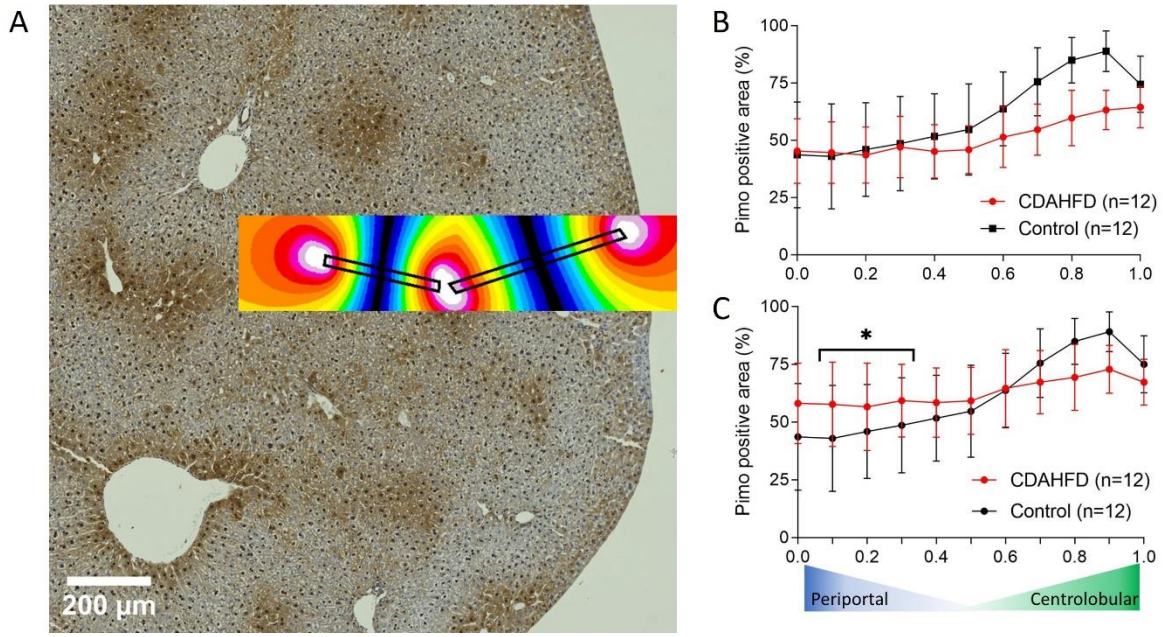

Figure 4.

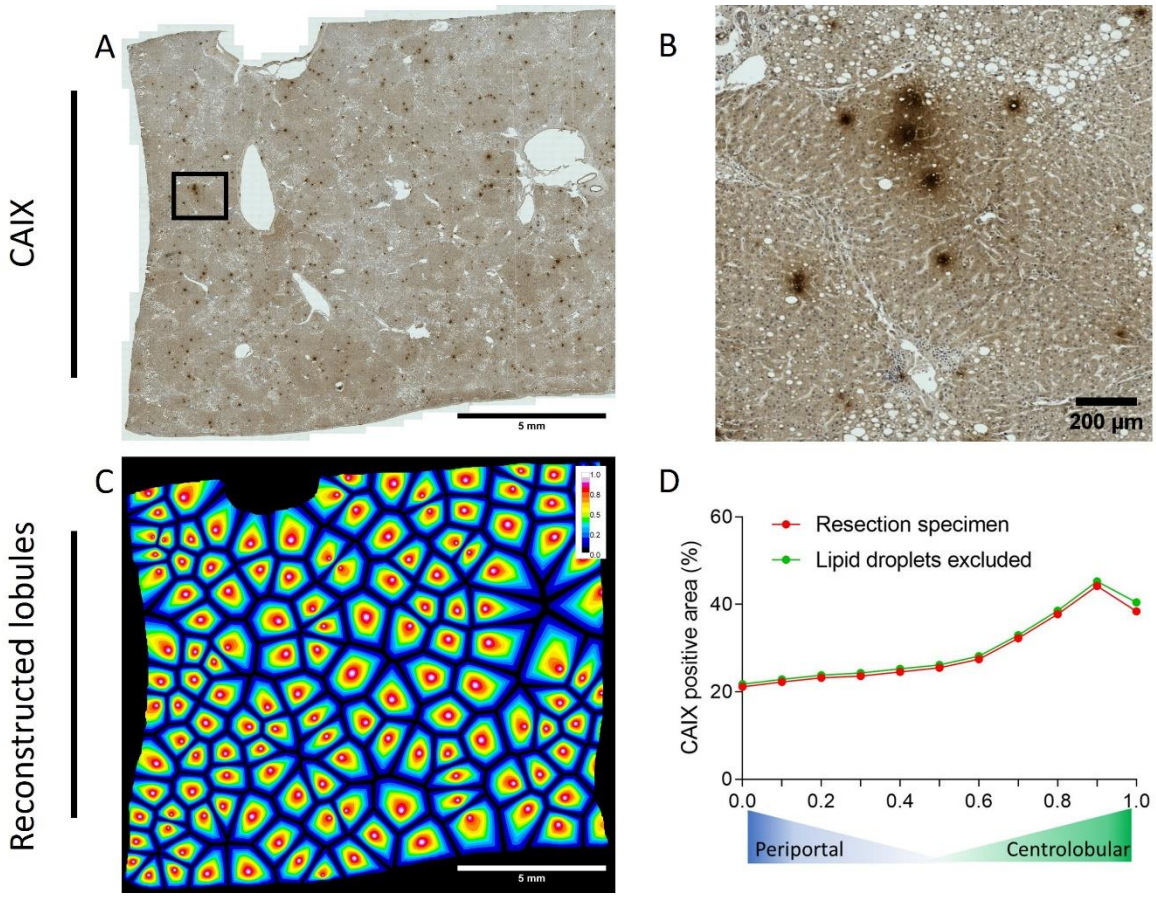

Figure 5.

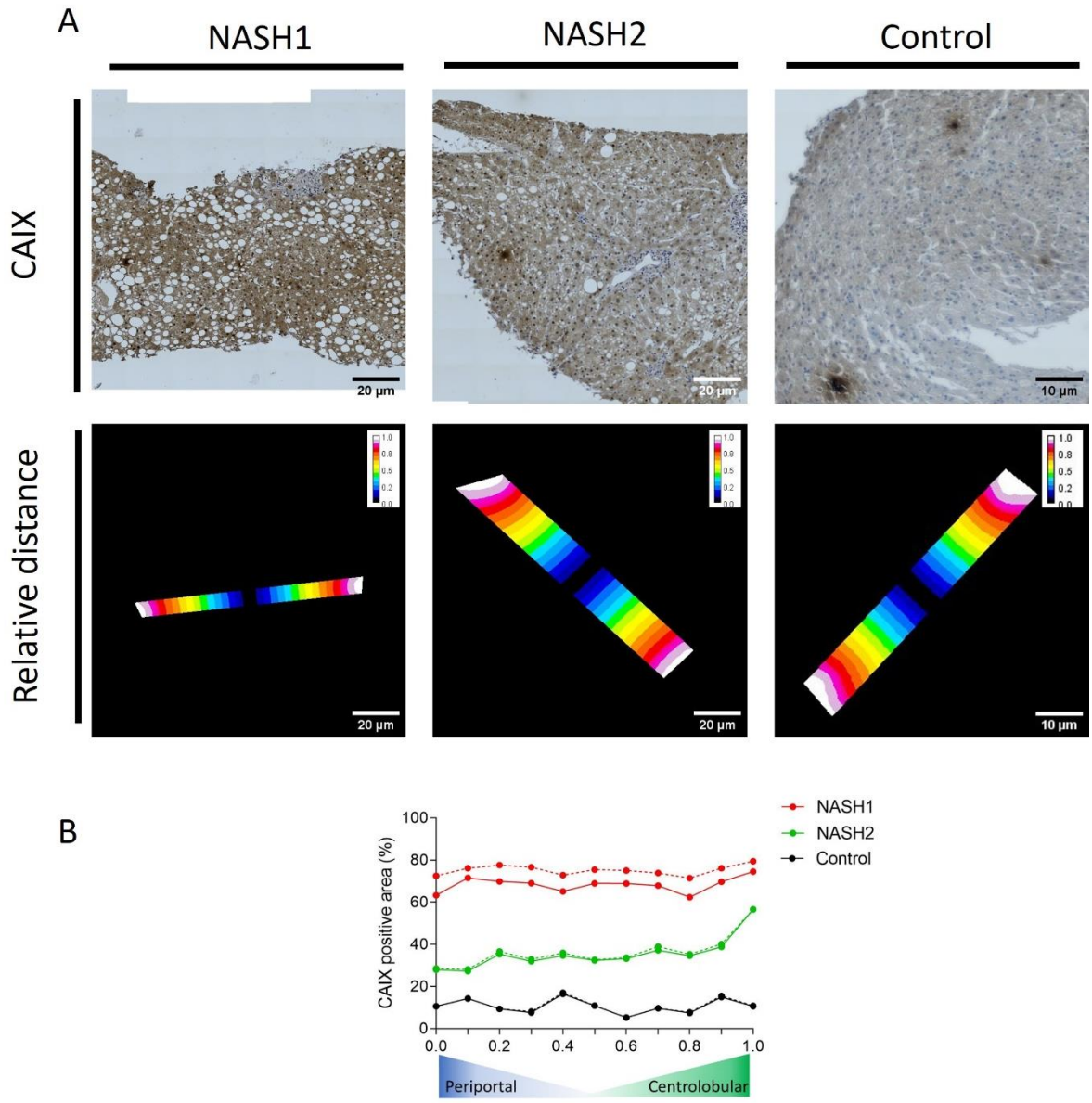
A
NASH1
NASH2
Control
CAIX
Relative distance
20 µm
20 µm
10 µm
20 µm
20 µm
10 µm
B
CAIX positive area (%)
100
80
60
40
20
0
0.0
0.2
0.4
0.6
0.8
1.0
Periportal
Centrolobular
NASH1
NASH2
Control

1

2